Study of small-amplitude magnetohydrodynamic surface waves on liquid metal

Hantao Ji,[a] William Fox,[b] and David Pace[c]
Plasma Physics Laboratory, Princeton University, Princeton, New Jersey 08543

H. L. Rappaport[d]
Institute for Fusion Studies, University of Texas at Austin, Austin, Texas 78712

(Received 11 May 2004; accepted 28 September 2004; published online 23 November 2004)

Magnetohydrodynamic (MHD) surface waves on liquid metal are studied theoretically and experimentally in the small magnetic Reynolds number limit. A linear dispersion relation is derived when a horizontal magnetic field and a horizontal electric current is imposed. Waves always damp in the deep liquid limit with a magnetic field parallel to the propagation direction. When the magnetic field is weak, waves are weakly damped and the real part of the dispersion is unaffected, while in the opposite limit waves are strongly damped with shortened wavelengths. In a table-top experiment, planar MHD surface waves on liquid gallium are studied in detail in the regime of weak magnetic field and deep liquid. A noninvasive diagnostic accurately measures surface waves at multiple locations by reflecting an array of lasers off the surface onto a screen, which is recorded by an intensified-CCD (charge-coupled device) camera. The measured dispersion relation is consistent with the linear theory with a reduced surface tension likely due to surface oxidation. In excellent agreement with linear theory, it is observed that surface waves are damped only when a horizontal magnetic field is imposed parallel to the propagation direction. No damping is observed under a perpendicular magnetic field. The existence of strong wave damping even without magnetic field suggests the importance of the surface oxide layer. Implications to the liquid metal wall concept in fusion reactors, especially on the wave damping and a Rayleigh–Taylor instability when the Lorentz force is used to support liquid metal layer against gravity, are discussed. © *2005 American Institute of Physics*. [DOI: 10.1063/1.1822933]

I. INTRODUCTION

The effect of a magnetic field and electric current on the dynamics of liquid metals with a free surface facing a vacuum or a nonconducting fluid (e.g., air), is a century-old problem, studied first by Northrup.[1] However, the progress in their understanding has been very limited, especially in the laboratory. Recently, a new interest has arisen in this problem, electrically conducting liquids, such as liquid lithium or liquid salt (Flibe), are proposed as the material facing the burning plasma in fusion reactors, directly handling the heat flux and breeding tritium from neutrons.[2–5] The Reynolds number of such flows is typically large ($\gtrsim 10^5$) due to the required fast flow rates, and the liquid is under extreme thermal stresses due to the high heat flux on the free surface.[2] A typical magnetic fusion reactor uses a strong magnetic field (on the order of 10 T) to confine plasma. Often, an electric current is driven in the conducting, plasma-facing material by either induction or an externally supplied voltage. In addition, unstable plasma modes can be coupled to free-surface modes of liquid wall.[6] A comprehensive understanding of dynamics of such liquids in magnetic fields and with applied currents becomes crucial for the success of this new application.

A first step towards this goal is to understand the physics of magnetohydrodynamic (MHD) surface waves[7] in a static pool subject to an externally applied magnetic field and a current parallel to the unperturbed surface. The past work on the subject, including theory and experiment, has been very limited. Murty[8] studied linear waves when the externally applied magnetic field and current are in the same direction. An instability due to the pinch force (the Lorentz force directed inward to the fluid) was found, consistent with the phenomena described by Northrup[1] when only the current was imposed. Similar instabilities in a current-carrying cylinder along an axial magnetic field were also studied.[9,10]

The first serious theoretical effort on a more general case, where the magnetic field has an arbitrary angle with current was made by Shercliff.[11] When the resultant Lorentz force is upward and is larger than gravity, the surface becomes unstable, as in the Rayleigh–Taylor instability. Earlier experiments had observed this instability.[12,13] Shercliff also found that a magnetic field and current introduces anisotropy in the propagation of surface waves. In addition, Shercliff estimated the effects of ohmic damping when the waves propagate parallel to the magnetic field. A similar theoretical study[14] was performed earlier on the subject but using more involved calculations. In both these studies, the magnetic field generated by the current was ignored so that the pinch instability was absent in the analysis.

[a]Electronic mail: hji@pppl.gov
[b]Present address: Physics Department, Massachusetts Institute of Technology, Cambridge, Massachusetts.
[c]Present address: Department of Physics and Astronomy, University of California, Los Angeles, California.
[d]Present address: Enig Associates, Inc., Silver Spring, Maryland 20904.

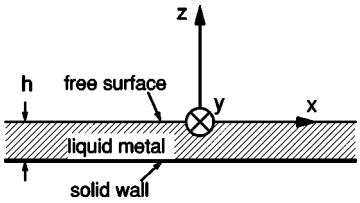

FIG. 1. The coordinate for surface wave analysis. The waves are assumed to propagate along x direction while the magnetic field and current are homogeneous and parallel to the free surface: $\boldsymbol{B}_0=(B_{0x},B_{0y},0)$ and $\boldsymbol{j}_0=(j_{0x},j_{0y},0)$.

Another assumption used by Shercliff was that the fluid velocity is two dimensional, restricted to the plane spanned by the vertical (gravity) and the vector of wave propagation. This assumption was relaxed only more than 20 years later by Shishkov[15] and Korovin.[16] While the former author did not elaborate on the consequences, the latter author claimed that the resultant dispersion relation and damping rate are significantly different except for some special cases.

Experimentally, there have been almost no quantitative studies of wave propagation and damping when a magnetic field or current is imposed parallel to the free surface. Experiments that we referred to earlier[1,12,13] focused on the pure growing mode due to the pinch force. The only published experiment found[17] used a magnetic field oscillating in time to simulate a perfectly conducting liquid metal facing to dc field.

Herein we report a detailed theoretical and experimental study of the propagation and damping of MHD surface waves on liquid gallium. Gallium was chosen simply due to its easy use for the intended experiments. We begin in Sec. II with a detailed derivation of the linear dispersion relation when both magnetic field and current are parallel to the free surface. It is found that the two-dimensional (2D) assumption made by Shercliff[11] does not impact the result, in contrast to the claims of Korovin.[16] In Secs. III and IV, we describe the experimental apparatus and results in detail. The dispersion relation and damping rates are measured and compared to the linear theory. Implications to the application of a liquid metal first wall in fusion reactors are discussed in Sec. V, followed by conclusions in Sec. VI.

II. LINEAR THEORY OF MHD SURFACE WAVES

A. Basic assumptions and governing equations

A flat layer of liquid metal with a free surface is assumed to be at rest sitting on top of a nonconducting wall with large horizontal dimensions compared to the layer thickness h. We define a Cartesian coordinate system as shown in Fig. 1, where surface waves are assumed to propagate along the x direction with a wave vector $\boldsymbol{k}=(k,0,0)$. Following Shercliff,[11] the externally imposed magnetic field and electric current are homogeneous and parallel to the free surface at rest: $\boldsymbol{B}_0=(B_{0x},B_{0y},0)$ and $\boldsymbol{j}_0=(j_{0x},j_{0y},0)$. Here, the subscripts 0 and 1 denote equilibrium values and oscillatory values in the wave, respectively.

An internal pressure profile $p_0(z)$ is set up to maintain static equilibrium ($\boldsymbol{V}_0=0$) by

$$\frac{\partial p_0}{\partial z}=-\rho g+j_{0x}B_{0y}-j_{0y}B_{0x}, \tag{1}$$

where ρ is the mass density of liquid metal and $g=9.8\ \mathrm{m/s^2}$ is the gravitational acceleration. Here, the magnetic field generated by the current flowing internally in the liquid metal B_{self}, which is on the order of $\mu_0 j_0 h$ is assumed to be negligible compared to the imposed B_0. (μ_0 is magnetic permeability of the vacuum and, by assumption, the liquid metal.) Ignoring the self-$\boldsymbol{B}$ field enforces the equilibrium Lorentz force $\boldsymbol{j}_0\times\boldsymbol{B}_0$ to be directed only vertically in the z direction, eliminating the pinch instability[8] discussed earlier. We note that this assumption is justified in the applications for fusion reactors, where the external magnetic field is typically strong and the needed external current, if any, is small. Assuming $j_0\sim\rho g/B_0$, an estimate is given by $B_{\mathrm{self}}/B_0\simeq\mu_0 j_0 h/B_0\simeq\mu_0\rho g h/B_0^2\simeq 3\times10^{-7}$ for the typical conditions[2] of $\rho=500\ \mathrm{kg/m^3}$ (lithium), $h=5$ mm, and $B_0=10$ T. This assumption is also well satisfied in the experiments reported later in this paper where no external current is imposed.

An important parameter characterizing dynamics of the liquid metal layer is the magnetic Reynolds number $R_{\mathrm{m}}=\mu_0 V h/\eta$ where V is a characteristic velocity and η is the electrical resistivity. For the present problem on surface waves in a static liquid metal layer, an appropriate choice for V is the phase velocity $V_{\mathrm{ph}}=\omega/k$, where ω is the angular frequency. For typical parameters available in the experiments described later $R_{\mathrm{m}}\sim10^{-2}\ll1$. In this small R_{m} limit, the wave-induced magnetic field is negligible, resulting in the so-called electrostatic approximation to Faraday's law $\partial\boldsymbol{B}_1/\partial t=-\nabla\times\boldsymbol{E}_1\approx0$ so the perturbing electric field must take the form $\boldsymbol{E}_1=-\nabla\phi$, while Ampère's law is replaced by $\nabla\cdot\boldsymbol{j}_1=0$. In addition, the wave-Lorentz force due to $\boldsymbol{B}_1$ is negligible, i.e.,

$$\frac{|\boldsymbol{j}_0\times\boldsymbol{B}_1|}{|\boldsymbol{j}_1\times\boldsymbol{B}_0|}\sim\frac{j_0}{B_0}\frac{\mu_0}{k}\sim\frac{\mu_0\rho g}{B_0^2 k}\simeq10^{-5}$$

using the aforementioned numbers with a wavelength on the order of 1 m.

As a result, linear waves in the liquid metal layer at rest ($\boldsymbol{V}_0=0$) are well described by a set of incompressible, inviscid but resistive MHD equations,

$$\rho\frac{\partial\boldsymbol{V}_1}{\partial t}=\boldsymbol{j}_1\times\boldsymbol{B}_0-\nabla p_1, \tag{2}$$

$$-\nabla\phi+\boldsymbol{V}_1\times\boldsymbol{B}_0=\eta\boldsymbol{j}_1, \tag{3}$$

$$\nabla\cdot\boldsymbol{j}_1=0, \tag{4}$$

$$\nabla\cdot\boldsymbol{V}_1=0, \tag{5}$$

where $\boldsymbol{V}_1$ and p_1 are the perturbed velocity field and pressure, respectively. In the momentum equation, the linearizing condition to ignore the convective derivative terms $\rho(\boldsymbol{V}_1\cdot\nabla)\boldsymbol{V}_1$ can be shown to be $ka\ll1$, where a is the amplitude of the surface displacement. ka is the wave "steepness." The linear theory is thus valid when the waves are not

steep; effects like breaking waves are inherently nonlinear phenomena where the steepness becomes infinite. Finally, note that every oscillatory quantity $f(t,x,z)$ can be assumed to take the form of $f(z)\exp[i(\omega t-kx)]$, where $f(z)$ is a function of only z. The boundary conditions shall be discussed in the following section.

B. Solving velocity and current fields

To satisfy the incompressibility condition, Eq. (5), the velocity field can be assumed to take the following shape

$$\boldsymbol{V}_1(x,z)=\boldsymbol{y}\times\boldsymbol{\nabla}\psi(x,z)+V_{1y}(x,z)\boldsymbol{y}, \tag{6}$$

so that $\boldsymbol{V}_{1x}=\partial\psi/\partial z$ and $V_{1z}=-\partial\psi/\partial x$. (Unlike Shercliff,[11] we include V_{1y} for the sake of completeness.) Using Eq. (6), Ohm's law, Eq. (3) or

$$\eta\boldsymbol{j}_1=-\boldsymbol{\nabla}(\phi-B_{0y}\psi)+V_{1z}B_{0x}\boldsymbol{y}-V_{1y}B_{0x}\boldsymbol{z}, \tag{7}$$

must satisfy Eq. (4) to yield

$$\eta\boldsymbol{\nabla}\cdot\boldsymbol{j}_1=-\nabla^2(\phi-B_{0y}\psi)-\frac{\partial V_{1y}}{\partial z}B_{0x}=0. \tag{8}$$

Since $\partial p_1/\partial y=0$, the y component of Eq. (2) simply becomes $\rho\partial V_{1y}/\partial t=(\boldsymbol{j}_1\times\boldsymbol{B}_0)_y=j_{1z}B_{0x}$, where j_{1z} is supplied by Eq. (7). Solving for V_{1y} yields

$$V_{1y}=-\frac{\partial(\phi-B_{0y}\psi)}{\partial z}\frac{B_{0x}}{i\rho\eta\omega+B_{0x}^2}. \tag{9}$$

Hence Eq. (8) is rewritten to a simple form of

$$\frac{\partial^2\Phi}{\partial z^2}=K^2\Phi,$$

where $\Phi\equiv\phi-B_{0y}\psi$ and $K^2\equiv k^2(1-iB_{0x}^2/\rho\eta\omega)\equiv k^2(1-i\alpha)$. Solving the above equation using the insulating boundary condition $(j_{1z}|_{z=-h}=0)$ or equivalently $j_{1z}|_{z=-h}\propto V_{1y}|_{z=-h}\propto\partial\Phi/\partial z|_{z=-h}=0$, yields the solutions for Φ

$$\Phi\equiv\phi-B_{0y}\psi=C\cosh[K(z+h)]\exp[i(\omega t-kx)], \tag{10}$$

where C is a constant.

A second equation is obtained through the y component of the curl of Eq. (2), $\rho\partial(\boldsymbol{\nabla}\times\boldsymbol{V}_1)_y/\partial t=[\boldsymbol{\nabla}\times(\boldsymbol{j}_1\times\boldsymbol{B}_0)]_y$, which reduces to

$$\rho\frac{\partial\nabla^2\psi}{\partial t}=B_{0x}\frac{\partial j_{1y}}{\partial x}=\frac{B_{0x}^2}{\eta}\frac{\partial V_{1z}}{\partial x}=-\frac{B_{0x}^2}{\eta}\frac{\partial^2\psi}{\partial x^2}$$

by using Eq. (7). Therefore, we again have

$$\frac{\partial^2\psi}{\partial z^2}=K^2\psi,$$

which can be solved by using the boundary condition $V_{1z}|_{z=-h}=-\partial\psi/\partial x|_{z=-h}=0$ to yield

$$\psi=A\sinh[K(z+h)]\exp[i(\omega t-kx)], \tag{11}$$

where A is a constant. With solutions for Φ and ψ given by Eqs. (10) and (11), the velocity, and current fields are known through Eqs. (6), (7), and (9) except the constants A and C

$$\boldsymbol{V}_1=\frac{\partial\psi}{\partial z}\boldsymbol{x}-\frac{1}{B_{0x}}\frac{\partial\Phi}{\partial z}\left(1-\frac{1}{1-i\alpha}\right)\boldsymbol{y}-\frac{\partial\psi}{\partial x}\boldsymbol{z}, \tag{12}$$

$$\eta\boldsymbol{j}_1=-\frac{\partial\Phi}{\partial x}\boldsymbol{x}-B_{0x}\frac{\partial\psi}{\partial x}\boldsymbol{y}-\frac{\partial\Phi}{\partial z}\frac{1}{1-i\alpha}\boldsymbol{z}. \tag{13}$$

C. Free-surface boundary conditions

Let $z=\delta(t,x)=\delta\exp[i(\omega t-kx)]$ represent the wavy free surface of the liquid metal. By definition,

$$\frac{\partial\delta}{\partial t}=V_{1z}|_{z=\delta}\approx V_{1z}|_{z=0}=-\left.\frac{\partial\psi}{\partial x}\right|_{z=0},$$

where "≈"represents linear approximation, again satisfied for small wave steepness. Thus

$$\delta=A\frac{k}{\omega}\sinh(Kh)\exp[i(\omega t-kx)]. \tag{14}$$

The second boundary condition on the free surface is that the current must be confined within the liquid metal, i.e.,

$$(\boldsymbol{j}_0+\boldsymbol{j}_1|_{z=0})\cdot\hat{\boldsymbol{n}}=0, \tag{15}$$

where $\hat{\boldsymbol{n}}$ is the unit normal vector of the free surface. Let $f=z-\delta$, then we have

$$\hat{\boldsymbol{n}}=\boldsymbol{\nabla}f/|\boldsymbol{\nabla}f|=iA\frac{k^2}{\omega}\sinh(Kh)\exp[i(\omega t-kx)]\boldsymbol{x}+\boldsymbol{z}.$$

Taking the first order of Eq. (15), we have $j_{0x}n_x+j_{1z}=0$ which becomes $C=iAj_{0x}K\eta/\omega$, leading to

$$\Phi=iA\frac{j_{0x}K\eta}{\omega}\cosh[K(z+h)]\exp[i(\omega t-kx)]. \tag{16}$$

D. Dispersion relation

Without losing generality, let the ambient pressure above the liquid metal be zero, which must balance with the pressure right underneath the surface plus a force due to surface tension,

$$p_1|_{z=0}+\left.\frac{\partial p_0}{\partial z}\right|_{z=0}\delta+T\frac{\partial^2\delta}{\partial x^2}=0,$$

where T is the surface tension coefficient. Thus, using Eq. (1), we have

$$p_1|_{z=0}=A\frac{k}{\omega}\sinh(Kh)(\rho g-j_{0x}B_{0y}+j_{0y}B_{0x}+k^2T)\times\exp[i(\omega t-kx)].$$

Applying this to the x component of Eq. (2),

$$\rho\frac{\partial V_{1x}}{\partial t}=-\frac{\partial p_1}{\partial x}-j_{1z}B_{0y}, \tag{17}$$

at $z=0$ yields the dispersion relation for MHD surface waves

$$\rho\omega^2=(\rho g+j_{0y}B_{0x}+k^2T)\frac{k^2}{K}\tanh(Kh), \tag{18}$$

where $K^2=k^2(1-i\alpha)$ and $\alpha=B_{0x}^2/\rho\eta\omega$.

A few observations on the above dispersion relation Eq. (18) are in order. First, setting $\boldsymbol{B}_0=\boldsymbol{j}_0=0$ recovers the usual surface wave dispersion relation in neutral fluid,

$$\rho\omega^2 = (\rho g + k^2 T)k \tanh(kh).$$

Second, the added imaginary component α due to the magnetic field along the propagation direction, will cause the surface wave to damp due to ohmic heating. A transverse magnetic field has no effect at all on the waves, because the perturbing motion does not bend field lines. The wave damping shall be discussed in detail in the later sections. Third, the second component of Lorentz force in the vertical direction $j_{0x}B_{0y}$ does not appear in the dispersion relation. The reason for the disappearance can be found in Eq. (17) where the second term on the right-hand side $-j_{1z}B_{0y}$ cancels the $j_{0x}B_{0y}$ term contained in the first term $-\partial p_1/\partial x$. Since the perturbed current j_{1z} arises because of the waviness of the free surface when a uniform current j_{0x} flows along the propagation (x) direction, this is a special effect due to the free surface facing a nonconducting fluid or vacuum. However, this effect leads to an instability (Rayleigh–Taylor instability) when the Lorentz force is used to put a liquid metal layer up against gravity in applications like in fusion reactor.[2] The detailed implications shall be discussed in Sec. V.

E. Deep liquid limit

The deep liquid limit, defined as $kh \gg 1$ when the wavelength is short, simplifies the dispersion relation by using $\tanh(Kh) \approx 1$ to

$$\rho\omega^2 = (\rho g + j_{0y}B_{0x} + k^2 T)\frac{k}{\sqrt{1 - i\alpha}}. \tag{19}$$

When B_{0x} is weak so that $\alpha \ll 1$ and $(1-i\alpha)^{-1/2} \approx 1 + i\alpha/2$, and if we assume that ω is real and k is complex, $k = k_r + ik_i$ ($k_r \gg k_i$), the real and imaginary parts of Eq. (19) give

$$\rho\omega^2 = (\rho g + j_{0y}B_{0x} + k_r^2 T)k_r, \tag{20}$$

$$k_i = -\frac{B_{0x}^2 \omega k_r}{2\eta(\rho\omega^2 + 2Tk_r^3)}, \tag{21}$$

respectively. The convective damping rate is given by Eq. (21), which reduces to simple $k_i = -(\alpha/2)k_r$ if $T = 0$. A small shortening of the wavelength enters in second order in α.

Here it is appropriate to provide a heuristic derivation of the damping rate Eq. (21). The ohmic dissipation is estimated as

$$\eta j^2 \simeq \eta\left(\frac{vB}{\eta}\right)^2 = \frac{v^2 B^2}{\eta},$$

where v is the characteristic fluid velocity. Then the wave energy decays as

$$\frac{\partial}{\partial t}\left(\frac{1}{2}\rho v^2\right) = -\frac{B^2}{\eta}v^2,$$

which leads to

$$a(t) = a_0 \exp\left[-\frac{B^2}{\rho\eta}t\right],$$

since $v = \partial a/\partial t = \omega a$. Setting $t = x/v_{\mathrm{ph}} = kx/\omega$ in the above equation leads to $a(x) = a_0 \exp(k_i x)$, where

$$k_i = -\frac{B^2 k}{\rho\eta\omega}.$$

This is consistent with Eq. (21) within a factor of 2 when the surface tension is ignored.

When B_{0x} is strong so that $\alpha \gg 1$, the dispersion relation relaxes to a different form,

$$\rho\omega^2 = (\rho g + j_{0y}B_{0x} + k^2 T)\frac{k}{\sqrt{2\alpha}}(1 + i). \tag{22}$$

If ω is set to be real and $T = 0$ for simplicity,

$$\rho\omega^2 = (\rho g + j_{0y}B_{0x})k_r\sqrt{\frac{2}{\alpha}},$$

$$k_i = -k_r,$$

which predicts that a strong magnetic field along the propagation direction shortens the wavelength, and, more importantly, leads to strong damping of surface waves within one wavelength. Note that the values of α are typically larger than unity in the fusion reactor application for parallel propagating waves while $\alpha \ll 1$ in the experiments reported in the following section.

F. Viscous effects

Viscosity has been ignored in the theory described so far because of its smallness. Here we estimate the viscous damping rate as following. Let v be characteristic fluid velocity due to the wave motion, then the dominant viscous force is given in deep fluids by

$$F_\nu = \rho\nu\frac{\partial^2 v}{\partial x^2} \sim \rho\nu k^2 v,$$

where ν is kinematic viscosity. Therefore, the wave energy decays as

$$\frac{\partial}{\partial t}\left(\frac{1}{2}\rho v^2\right) = -F_\nu v = -\rho\nu k^2 v^2,$$

which leads to

$$a(t) = a_0 \exp(-\nu k^2 t), \tag{23}$$

since $v = \partial a/\partial t = \omega a$. We note that Eq. (23) is consistent with more rigorous derivations[18,19] within a factor of 2. Setting $t = x/v_{\mathrm{ph}} = kx/\omega$ in Eq. (23) leads to $a(x) = a_0 \exp(k_i x)$, where

$$k_i = -\frac{\nu k^3}{\omega}. \tag{24}$$

Since viscosity for liquid metal is typically small,[20] the normalized viscous damping rate k_i/k is small. For liquid gallium, k_i/k is on the order of 10^{-4} (see later).

There is also a viscous drag effect due to the friction between the oscillating fluid and stationary tank boundaries.[18] Landau and Lifshitz calculate the temporal damping rate to be

$$\gamma = \frac{1}{2\sqrt{2}} \frac{2h+w}{wh} \sqrt{\nu\omega}, \tag{25}$$

which depends the fluid depth h, and the tank width w. This calculation requires that the viscous effects be confined to a narrow boundary layer near the walls, small enough so as not to change the dispersion relation calculated assuming ideal fluid motion at the boundary, i.e., that the boundary layer thickness is much less than the depth. This requirement is well satisfied: the width of the boundary layer is of the order $\sqrt{\nu/\omega} \lesssim 10^{-2}$ cm, negligible compared to the typical depth of 1 cm. Regarding the dissipation formula, as might be expected, since the damping gives the energy dissipated per unit energy in the fluid, and all the energy dissipation occurs at the boundary, the expression incorporates the ratio of the area of contact with the wall ($2h+w$ per unit length) to the fluid volume (wh per unit length). For liquid gallium, k_i/k is estimated to be on order of 10^{-3} (see later), which is still small.

G. Summary of linear theory of MHD surface waves

A short summary on theory of the linear MHD surface waves with horizontal magnetic field and current is in order before describing detailed experimental apparatus and results. In the small magnetic Reynolds number limit or when the induction is negligible and the self-field due to imposed electric current is small, the wave dispersion is given by Eq. (18). Only the component of the Lorentz force with parallel B and perpendicular j contributes to the dispersion (this is due to a cancelling of j_{0x} by j_{1z}, which arises to keep the current confined to the gallium surface). As a result, a magnetic field perpendicular to the propagation direction affects neither the wavelength nor damping of surface waves. A parallel magnetic field damps waves in liquid with depth on the order of a wavelength and deeper while viscous damping is small. The magnetic damping efficiency depends on the dimensionless parameter $\alpha = B_{0x}^2/\rho\eta\omega$ and the waves are weakly damped when $\alpha \ll 1$ and strongly damped when $\alpha \gg 1$.

Next, experimental studies of MHD surface waves in a table-top device are described in detail. The experiments do not cover the full parameter regimes in which the theory is valid. More specifically, the experiments are limited to the cases when no current is imposed and $\alpha \ll 1$ in the deep liquid limit. The small magnetic Reynolds condition is always satisfied.

III. EXPERIMENTAL APPARATUS

We have constructed an experiment to study the properties of liquid gallium surface waves in an applied magnetic field. Figure 2 illustrates the major components of the experimental apparatus: the gallium tank, wave driver and paddle, magnetic field coils, and surface diagnostics. A noninvasive diagnostic measures the waves by reflecting multiple laser beams off the surface and onto a screen, which is filmed by a camera. A PC-based Labview program with a National Instruments PCI-1671E board controls the experiment by controlling the magnetic field strength, gathering data, gating the wave driver, and digitizing the images from the camera. Below we briefly describe each component of the above experimental apparatus; a more detailed discussion of the experimental setup, including photographs, can be found in one of the author's Bachelor thesis.[19]

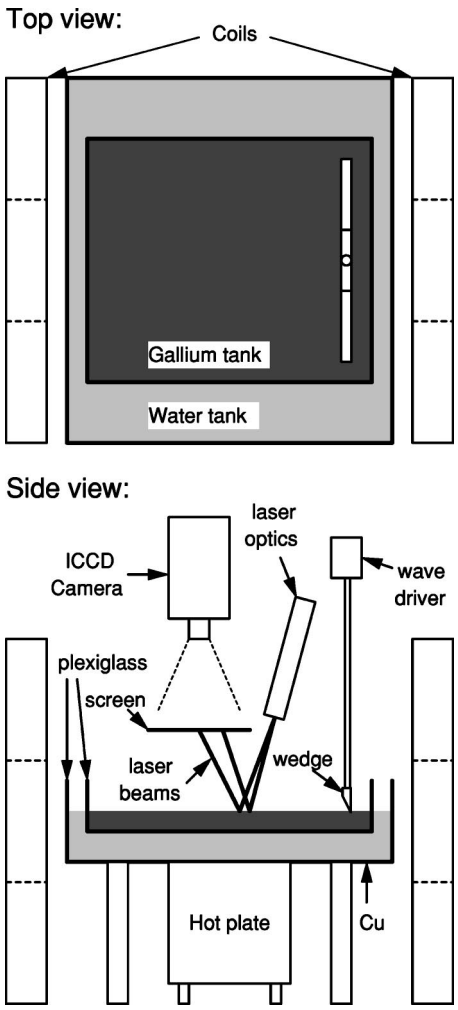

FIG. 2. Experimental setup for study of MHD surface waves in liquid gallium: top view (top panel) and side view (bottom panel).

A. Gallium tank

Gallium, which melts at a low temperature of about 30 °C, is believed to be nontoxic, and the oxidation is confined to a skin layer. It is an ideal metal for table-top liquid metal studies than other candidate metals such as mercury,[21,22] which is highly toxic and has a high vapor pressure, and lithium and sodium, which are reactive with water.[2,23] Approximately 1400 cc of gallium is held in a square plexiglass tank which has a side length of 37.8 cm and a height of 5 cm. The depth of the gallium layer is about 0.9 cm, which satisfies the condition for the deep liquid limit for the most cases in our experiments. The size of the tank is constrained by the cost of gallium, but must be large enough

to minimize boundary effects. The gallium tank sits in a larger water tank, which serves as a heat reservoir. (Gallium has about 1/10 the specific heat of water.) The water tank, which has a copper bottom plate, is in turn heated from below by a hot plate (by Thermolyne Corp. Model 5PA10258); the water temperature was monitored with a thermocouple.

In finding a minimum width of the gallium tank in the y direction, a few characteristic lengths need to be considered. The first length concerns the thickness of viscous boundary layers, which is only on the order of $\sqrt{\nu/\omega} \sim 10^{-2}$ cm. Second, there is a characteristic length for the wave-induced current in the y direction [see, e.g., Eq. (13)] j_{1y} to return at the side boundaries. Because of small R_m or large resistivity, the current return areas are expected to extend from the side walls for about half a wavelength, a distance over which j_{1y} reverses its direction. Since the longest wavelength in our experiments is about 6 cm (see later), this characteristic length is about 3 cm. Finally, the tank width should be much longer than the capillary length, $\sqrt{T/\rho g} \sim 0.34$ cm. However, the capillary boundary effects are more pernicious, and, in fact, the tank must be made as wide as possible. The gallium generally does not wet the plexiglass walls evenly, and the nonuniform meniscus at the boundaries scatters the single incident waves and creates nonplanar waves, and interference, downstream. Thus, in contrast to larger water wave experiments (with flumes less than meter wide and tens of meters long), this small gallium experiment is nearly square in aspect ratio.

The end boundary also needs special attention. Since our aim was to observe traveling waves, one possibility is to find some boundary at the far end that simulates an infinite tank, such as impedance matching on a transmission line. Reflections from the end boundary (opposite the side from which waves are driven) complicate the patterns on the surface, and the seven-point laser diagnostic we used does not adequately resolve the counter-propagating waves. In the end, it is found that the best way to make a precise measurement of the wave is to use transient data, taken before reflected waves could return to the measurement location.

B. Wave driving hardware

The paddle design is another way in which this experiment deviates from larger hydrodynamics experiments. While those experiments use large paddles hinged to the bottom or large wedges to drive waves, early tests we conducted in water and gallium found that wedge-type wave drivers caused splashing if the wedge angle is large (45°). For the experiments reported here, we used a wedge with a smaller angle of 31° or an edge of 1/16 inch copper sheet. Unlike the wedge-type paddles, which drive waves by moving volumes of fluid, this kind of paddle pulls up and down on the surface with surface tension. Both paddles were about 34 cm wide, about 90% of the width of the tank. To drive planar waves with a single $\mathbf{k}$, it is very important to have uniform contact along the length of the paddle. When setting up experiment runs, it was important to optimize the planarity of the waves, which we checked using the laser diagnostic described below.

The paddle motion is driven in by the wave driver, an electromechnical device (Mechanical Vibrator SF-9324 from Pasco Scientific) similar to a speaker, but more robust and magnetically shielded. The input sinusoid comes from a signal generator, gated by the experiment control, through a power amplifier. Prior to experiments using gallium, the wave driving hardware was tested using water with and without magnetic field. It was found that the driven waves in water were not affected by presence of a magnetic field, confirming that the wave driving hardware is insensitive to the magnetic field.

C. Magnetic field coils

In our experiment we have used two pairs of "L-2" coils in a magnetic mirror configuration to provide a relatively uniform, dc magnetic field. The coils, of outer diameter 49.8 cm, are separated by 50.8 cm. Currents of up to 500 A create a field of up to $B_0 = 400$ G at the center in between the coils. Because the gallium tank sits in the midplane of the coils, there is no vertical component to the magnetic field at the liquid surface.

D. Laser surface diagnostic

To measure the surface waves, we reflect lasers off the surface and onto a screen filmed by an ICCD (intensified charge-coupled device) camera (by ITT Corp.). A passing wave distorts the local angle of the gallium surface and perturbs the laser spot on the screen from its flat-surface position. When the wave amplitude a is small, the deflection of the laser spot is proportional to the slope of the passing wave; the diagnostic thus directly measures the wave steepness ka, where k is the wave number. Measuring the relative phases of multiple points on the surface determines the wave number k, and where a.

The experiment, once configured, is triggered off of a camera gating pulse. Thus, the camera frames correspond to exactly the same points in time in each experiment, confirming that the experiments are highly repeatable. A similar technique was implemented in a recent experiment on (non-MHD) surface wave in mercury.[24]

The diagnostic consists of a laser rail, on which the laser (2 mW, He-Ne by Uniphase Model 1101P), and associated optics are mounted, a screen near the gallium surface, and an ICCD camera. Following optics to focus the laser spot on the surface, a diffracting beam splitter (a dot-matrix projection head from Edmunds Optics) splits the laser beam into a diverging matrix of beams, and a mask blocks all but the central row of up to seven beams. The resultant beams lie in a plane, whose intersection with the plane of the gallium surface is a line parallel to the direction of wave propagation.

The camera takes 60 frames per second (de-interlaced), which are digitized by a National Instruments NI-1407 series frame grabber board and saved to disk. The image intensification hardware on the camera allows for controlled gating of the exposure time; typically, gate widths of 100 μs–1 ms were sufficient to freeze the laser spot in each frame.

We now present a way to map the laser spot measurements back to the wave motion, valid for small-amplitude

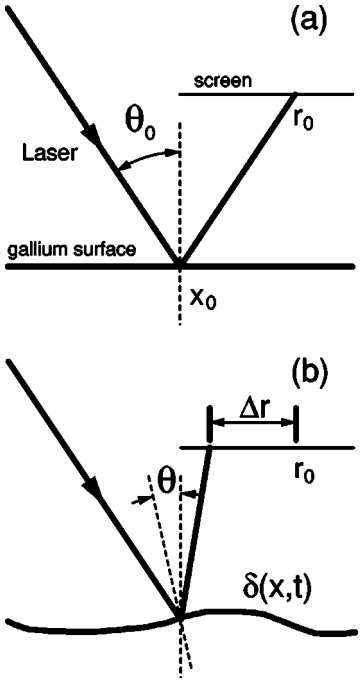

FIG. 3. Laser reflection from the fluid surface (a) flat surface and (b) surface with waves.

waves and diagnostic laser beams that come in close to vertical. Figure 3(b) shows a picture of the laser reflection in the x-z plane for waves propagating in the x-direction.

Figure 3(a) shows a schematic picture of a laser reflecting from a flat surface at x_0 and intersecting the screen at the position r_0. When a wave passes, the angle of the surface changes and the laser spot shifts to $r_0+\Delta r$. We now correlate the motion of the spot on the screen $\Delta r(t)$ with the motion of the free surface $\delta(x,t)=a\ \sin(kx-\omega t)$.

The angle of incidence of the laser beam, θ_0, will be a different value for each of the seven incident laser beams, because the beams diverge from one another. It will however, be treated as small; the largest incident angle was 4°. We discuss below how to precisely calibrate the θ_0's from a few simple, *in situ* measurements. The flat-surface position of the laser spot on the screen is $r_0=x_0+d\ \tan(-\theta_0)$, where d is the distance of the screen from the gallium surface.

In general, a passing wave not only changes the angle that the ray reflects off at, but also changes the position where the ray intersects the surface, and thus the surface point that the laser samples. However, this effect can be neglected in the first order, as discussed below. In this first approximation of small θ_0 and wave amplitude, the laser always reflects off the surface at the point $(x,z)=(x_0,0)$. The surface normal at this point due to traveling waves is $\mathbf{n}(t)=\boldsymbol{\nabla}[z-\delta(x,t)]=[ka\ \cos(kx_0-\omega t),0,1]$. (The laser rays also have a finite component in the y direction. However, the projection of the incident and reflected rays onto the x-z plane does not depend on it.) Let θ be the inclination of the surface normal, $\tan\theta(t)=ka\ \cos(kx_0-\omega t)$.

With this definition of θ and θ_0, simple geometry shows that the angle of reflection is $2\theta-\theta_0$. Thus, the motion of the spot on the screen will be

$$\Delta r(t) \approx d\ \tan(2\theta-\theta_0)-d\ \tan(-\theta_0) \approx 2dka\ \cos(kx_0-\omega t), \tag{26}$$

if $\theta\sim ka\ll 1$ and $\theta_0\ll 1$. The factor kx_0 affects the phase of the laser motion on the screen. Since the reflection positions $\{x_0\}$ can be precisely calibrated, it is possible to experimentally measure k by comparing the phases of the seven laser spots.

We now discuss the lowest order corrections to these formulae. First, in the expression above we have used small-angle approximations for the tangent; thus corrections to the above formula will be proportional only to second-order products of ka and θ_0. We also introduce errors by assuming that the reflection always occurred at $(x_0,0)$. The next approximation of the reflection point is $[x_0-\delta(x_0,t)\theta_0,\delta(x_0,t)]$. The small shift of the reflection position has two effects: first, there will be a correction to the surface normal, and second, the laser will reflect from a different surface height. The former can be evaluated from a Taylor expansion of the surface normal about x_0,

$$n_x \approx n_{x_0}+\left.\frac{\partial n_{x_0}}{\partial x}\right|_{x_0}(x-x_0).$$

The correction to the above formula (26) is therefore of order $ka\theta_0$, since taking the derivative of δ is proportional to k and the position shift is of order $a\theta_0$. This correction, then enters at the same order as the corrections to tangent. Next, the second finite amplitude effect changes the total distance the laser travels, shifting the position of the spot on the screen by about $2\delta(t)\tan\theta_0\approx 2a\theta_0$. Comparing this to our linear formula (26), we can see the correction is of order a/d, which is small in our setup: $a\sim 0.1$ mm while $d\sim 10$ cm.

E. Calibrations

To calibrate the laser diagnostic, first the beam splitter was carefully characterized to determine the interbeam divergence. Once this is known, a few still frames taken with the laser in place in the experiment is sufficient to calibrate the angle θ_0 of each ray and the height of the screen, to better than 1%. The first still frame is taken with the screen moved intersect the beams on the way to the gallium. The second is taken with the screen in its normal position, so that the laser beams intersect the screen after reflecting off the flat gallium surface. The difference in laser spots between the two frames is only due to the path of the lasers between the plane of the screen and the plane of the gallium surface. From knowledge of the interbeam divergence and these measurements, one can determine the height of the screen, the angle θ_0 of each laser, and the location on the surface that each laser measures. Finally, a still frame taken of a grid of points in place of the screen maps pixels to real-world units and in principle allows for correction of any optical distortion in the camera optics. (We did not, however, observe any distortions in our optical setup.)

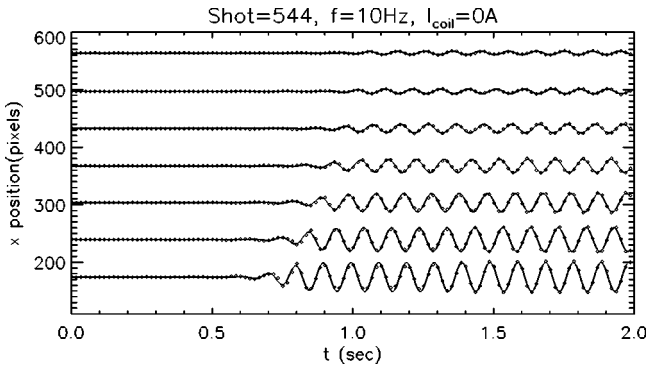

FIG. 4. Examples of measured movements of reflected laser spots on the screen as functions of time (diamonds). Solid lines indicate fitted curves to the measurements (see text).

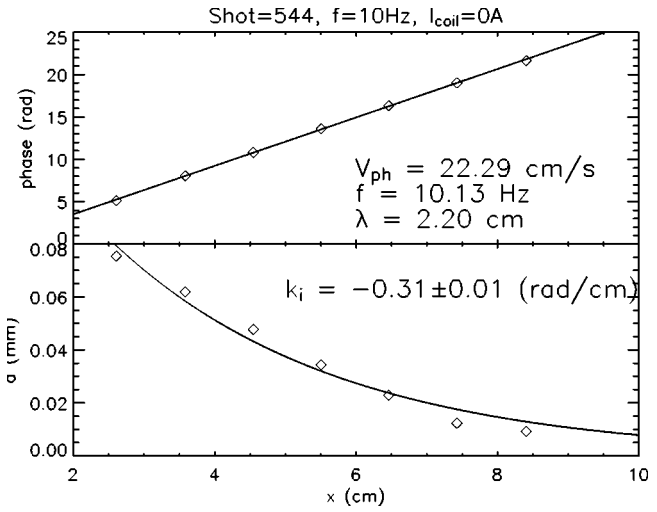

FIG. 5. The wave phase (top) and amplitude (bottom) as functions of x for the example given by Fig. 4. The uncertainty of each point is smaller than the symbol size.

F. Procedures for data analysis

The camera takes images of the laser spot motion, which are digitized and saved. For analysis, an IDL (interactive data language) program was written to find the laser spots in each frame, by finding the regions with the brightest points. The location of the spot is determined consistently by a mass-weighted average of the light intensity over a small region containing the spot, after removing background light. The error in the location of the spot center is assigned to be 1 pixel (since the centroid is determined more accurately than this). As mentioned before, because we can control the camera shutter gating, we can gate for a short enough time so that the laser spots do not smear in the frames.

After finding the lasers in each frame, a time series of spot motion is assembled at each surface location. It is found that a sinusoid is an excellent fit to each time series, consistent with Eq. (26). From the fitting parameters, we can find the frequency, relative phase of the spots, and the amplitude of the spots motion, from which we find ka at each surface location.

IV. EXPERIMENTAL RESULTS

Descriptions of experimental results are divided into two sections: wave propagation and wave damping, which correspond to the real and imaginary parts of the dispersion relation, respectively, as exemplified by Eqs. (20) and (21) in the deep liquid and weak magnetic field limits. Discussions are included in each section following the descriptions of results.

A. Wave propagation without magnetic field

Figure 4 shows an example of the measured movements of seven reflected laser spots on the screen as functions of time. We focus on waves in the early times after the initiation before they are reflected from the end boundary to minimize the effects due to standing waves (see Sec. III B). The movement of each reflected laser is fitted to the function of

$$\Delta r(t) = \frac{1}{2}\left(\tanh\frac{t-t_0}{\tau}+1\right)\Delta r_0 \sin(\omega t - p) + c, \tag{27}$$

where all parameters except t are fitting parameters. Here t_0 represents the arriving time of the waves at each laser and Δr_0 is related to the wave amplitude by Eq. (26),

$$\Delta r_0 = 2dka. \tag{28}$$

The fitting is performed by a nonlinear fitting procedure provided by the IDL package, and the fitted curves are shown by solid lines in Fig. 4. The wave frequency $f=\omega/2\pi$ is accurately determined the fitting and is 10.13 ± 0.03 Hz for the example given by Fig. 4. The wave phase p is fitted linearly with position x as shown as the solid line in Fig. 5 (top), and the slope of the line determines the wave number k or equivalently the wavelength λ which is 2.20 ± 0.01 cm for the example given by Fig. 4. Consequently, the wave amplitude at each laser is determined by Eq. (28) since all other quantities $(\Delta r_0, d, k)$ are known. The obtained amplitudes are shown in Fig. 5 (bottom).

In order to measure the dispersion relation of the MHD surface waves, the driving frequency is varied from about 4 Hz to about 12 Hz. The lower frequency is limited by the size of the gallium tank which can only accommodate few wavelengths at lower frequencies. The upper frequency is limited by the time resolution of frame acquisition rate of 60 Hz. While there is no Nyquist frequency *per se*, because the waves are monochromatic and the wave frequency is approximately known, the fitting routine used still requires good time resolution to converge.

The measured dispersion relation with no imposed magnetic field is shown in Fig. 6 as diamonds, which is compared with theoretical predictions by Eq. (18) with $j_{0y}=B_{0x}=0$,

$$\rho\omega^2 = (\rho g + k^2 T)k \tanh(kh) \tag{29}$$

using the published value of surface tension coefficient[20] (solid line). Agreement is found between experiment and theory only for the low frequencies, but not for high frequencies. The measured wavelengths are shorter than predicted values for a given driving frequency. However, an *ad hoc* surface tension coefficient, lowered by a factor of 2.5, agrees fairly well with the experiment at all frequencies.

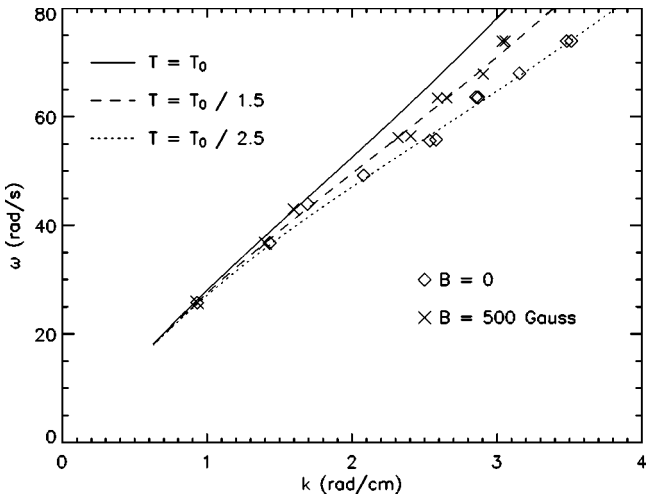

FIG. 6. The measured dispersion relation of MHD surface waves in gallium without magnetic field (diamonds) and with $B_0=380$ Gauss (cross). Theoretical curves by Eq. (29) are shown for three cases: $T=T_0=0.718$ N/m (solid line); $T=T_0/1.5$ (dashed line); and $T=T_0/2.5$ (dotted line).

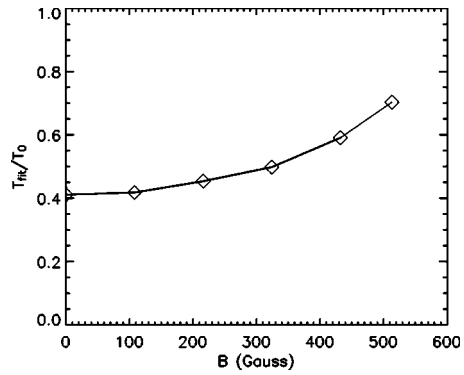

FIG. 7. The fitted surface tension coefficient normalized by published value (Ref. 20) for clean gallium $T_0=0.718$ N/m as a function of imposed magnetic field.

The validity of direct comparisons of "transient "waves (Fig. 5) with the theoretical predictions [Eq. (29)] derived under the assumption of continuous waves deserves some discussions here. Recall that the quantity ω^2 in Eq. (29) originates from the second time derivative of a continuously oscillatory wave: $z''=-\omega^2 z$ where $z=a\ \exp[i\omega t]$. Like Eq. (27), a transient wave can be expressed as

$$z=\frac{1}{2}\left(\tanh\frac{t}{\tau}+1\right)a\ \exp[i\omega t],$$

without losing generality. After some algebra, the second time derivative is given by

$$z''=-\omega^2 z\left[1+\frac{2}{\omega^2\tau^2}\frac{\mathrm{sech}^2(t/\tau)\tanh(t/\tau)}{\tanh(t/\tau)+1}-\frac{2i}{\omega\tau}\frac{\mathrm{sech}^2(t/\tau)}{\tanh(t/\tau)+1}\right],$$

where typically $\omega\tau=2\pi f\tau\gg 1$ as evident in Fig. 5. When $t\ll\tau$, the above equation leads to an angular frequency of $\omega-i/\tau$, which represents a "growing"wave around $t=0$. When $t\gg\tau$, the above equation reduces to

$$z''=-\omega^2 z\left[1+\frac{4}{\omega^2\tau^2}\exp\left(-\frac{2t}{\tau}\right)-\frac{4i}{\omega\tau}\exp\left(-\frac{2t}{\tau}\right)\right].$$

The correction terms to ω are very small ($\lesssim 10^{-4}$) since typically the data at least up to $t=5\tau$ are used. Therefore, the continuous wave assumption is justified for the transient data described here.

The apparent reduction of surface tension is likely due to a thin oxide layer formed on the gallium surface. The oxide layer becomes visible when a clean liquid gallium is exposed to air for a few hours if left still, or appears in only a few minutes if surface waves are driven. A decrease in surface tension due to oxidation is qualitatively consistent with a small chemistry experiment performed by the authors. After covering of small blob of gallium with a coating of 1 mole hydrochloric acid solution, the surface became very shiny as the acid cleaned the oxide layer from the surface. At the same time the surface was cleaned, the gallium pulled itself up into a tight ball, implying increased surface tension. Later, as the acid evaporated and the surface reoxidized, the gallium lost its uniform tight shape, implying that the surface tension decreased. In addition, attempts to keep the surface free of oxidation were made by displacing oxygen with pure nitrogen and argon gases, however, without apparent success. According to separate experiments[25] to study surface atomic physics of pure gallium, controlled oxidation can be achieved only under ultrahigh vacuum with a base pressure of 10^{-9} Torr and an oxygen partial pressure of 10^{-11} Torr. These conditions were not available for the experiments reported here.

B. Wave propagation with magnetic field

The effects of a horizontal magnetic field on the surface wave dispersion relation are studied by repeating the above experiments with varying strength of the applied field. Also shown in Fig. 6 are the results obtained under a parallel imposed field of $B=500$ G at the measurement locations. At a given driving frequency, the wavelength is observed to increase with B. At $B=500$ G, the lengthened wavelength is still shorter than the predictions using $T=T_0$, but the observed changes are more than 10% at $f\approx 12$ Hz. Interestingly, the measurements agree well with the predictions using $T=T_0/1.5$. To quantify the observed changes better, the measured dispersion relation is fitted by Eq. (29) with T as a free parameter. The fitted T is shown as a function of B_x in Fig. 7.

The observed change in the dispersion relation of the surface wave propagation due to magnetic field cannot be simply explained by linear theory. According to Eq. (18), the real part of the dispersion relation does not depend on magnetic field if the dc current density is zero. This is better seen in Eq. (29), which is valid in the limit of weak magnetic field ($\alpha=B_{0x}^2/\rho\eta\omega\ll 1$), a condition well satisfied in our experiments. For example, for $f\approx 12$ Hz and $B=500$ G, $\alpha=0.022$. The next order corrections to the dispersion is on the order of $\alpha^2\approx 5\times 10^{-4}$, which is much smaller than the measured changes. Furthermore, the observed changes cannot be ex-

plained by nonlinear effects, which is on the order of the ratio of $\rho(\boldsymbol{V}_1\cdot\boldsymbol{\nabla})\boldsymbol{V}_1$ to $\rho\partial\boldsymbol{V}_1/\partial t$ (see Sec. II A) or simply $ka\sim 10^{-2}$. The effect due to omission of the wave-induced magnetic field $\boldsymbol{B}_1$ is also small

$$\frac{B_1}{B_0}\sim\frac{\mu_0 j_1}{kB_0}\sim\frac{\mu_0 V_1}{k\eta}\sim\frac{\mu_0\omega a}{k\eta}\sim 6\times 10^{-5}.$$

We therefore seek explanations outside of the physics in the linear MHD dispersion relation. One possible explanation of the observed changes in effective surface tension force with an imposed magnetic field is changes in atomic physics in the surface oxide layer or the adjacent pure gallium layers. The structure of surface of liquid metal has been a hot topic in recent years, especially after rapid development of experimental techniques, such as x-ray reflectivity measurements, to directly study the surface structure. A recent review paper is given by Penfold on this topic.[26] A theoretically predicted phenomenon called surface-induced atomic layering[27] due to the sharp discontinuity in density across a liquid-vapor surface has been confirmed experimentally.[25] The effect of oxidation on the liquid gallium free surface has also been studied[28] by x-ray scattering. It was found that the oxide layer has a uniform thickness of about 5 Å, which does not increase with further oxygen exposure and temperature increase. The dependence of these surface properties on the magnetic field has been reported neither experimentally nor theoretically. However, it would not be surprising to have some dependences on magnetic field since liquid gallium has larger degrees of covalency (less close to a free-electron metal) and directional bonding.[26] We should note that the dispersion relation remains unchanged when the magnetic field is imposed horizontal but perpendicular to wave propagation.[19] This fact constrains a theory of surface tension modification by a magnetic field: the magnetic field can only modify the surface tension along the direction of the magnetic field.

C. Wave damping without magnetic field

The linear theory predicts that waves interact with a parallel magnetic field, leading to damping in deep fluids [Eq. (21)]. However, as shown in Fig. 5, wave damping exists even without magnetic field. To quantify the wave damping rate, the amplitudes are fitted to the function of

$$a(x) = a_0\,\exp[k_i(x-x_0)], \tag{30}$$

where a_0 and k_i are fitting parameters and x_0 is the x position of the first laser measurement. The magnitude of k_i characterizes the damping rate. The fitted curve is also shown in Fig. 5, where the error in k_i, δk_i, is estimated by equating the measurement uncertainties $\delta a(x)$ to $a_0(x-x_0)\exp[k_i(x-x_0)]\delta k_i$. (One should note that there exist also systematic errors in k_i due to deviations from the perfect e-folding beyond statistical uncertainties in the measurements. Using residual fitting errors, the systematic errors in k_i are estimated to be about four times larger than the statistical counterparts.) Figure 8 shows that the normalized damping rate k_i/k, increases with k, but saturates at about 0.1 at large k.

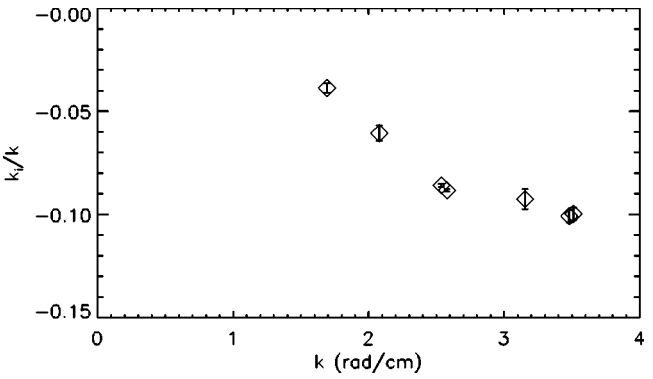

FIG. 8. The normalized wave damping rate k_i/k vs k without magnetic field.

Absent a magnetic field, waves can be damped by finite viscosity, which has been ignored in the linear theory described earlier because of its smallness. The normalized damping rate due to bulk viscous forces is estimated via Eq. (24),

$$\frac{k_i}{k} = -\frac{\nu k^2}{\omega}\simeq -(1-4)\times 10^{-4},$$

using the published value[20] for gallium viscosity $\nu\simeq 3\times 10^{-7}\mathrm{m}^2/\mathrm{s}$ and the measured values for other quantities. The damping rate due to boundary viscous layers can be estimated via Eq. (25)

$$\frac{k_i}{k} = -\frac{1}{2\sqrt{2}}\frac{2h+w}{wh}\sqrt{\frac{\nu}{\omega}}\simeq -(2-4)\times 10^{-3},$$

which is larger than that due to bulk viscous effects, but it, too, is too small to explain the observed wave damping without magnetic field.

An alternate explanation again can be based on existence of the surface oxide layer, which has been described in Secs. III A and III B. It was found from the x-ray scattering experiments[28] that the thermal capillary waves, which limits the x-ray reflectivity at higher temperatures on an unoxidized gallium surface, were largely suppressed by oxidization. This suggests that the oxide layer is a solid phase, and other spectroscopy showed that the oxide layer is amorphous, suggesting that the oxide layer is rigid but not elastic, and can cause wave damping. Qualitatively, it was observed that the gallium surface becomes less excitable as the oxide layer forms. In fact, deviations from the exact exponential decay, as seen in Fig. 5, may be due to nonuniformness of the oxide layer, which often is visible. We note that in general the wave damping due to this mechanism can also depend on the wave amplitude, and this effect was not investigated in our experiment (Fig. 8). On the other hand, quantitative theoretical estimates are not possible without detailed knowledge of physical properties of the layer, which is beyond the scope of the present paper.

D. Wave damping with magnetic field

According to the linear theory described in Sec. II, MHD surface waves in the deep liquid limit are not damped by a perpendicular magnetic field to the propagation direction, but

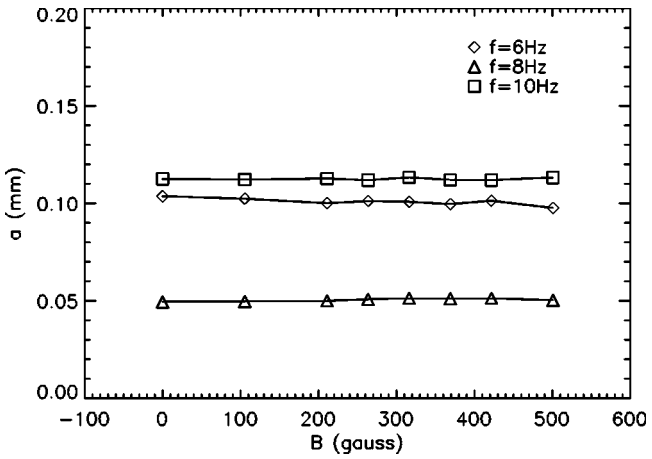

FIG. 9. The wave amplitude measured by the first laser as a function of magnetic field perpendicular to the propagation direction for several frequencies.

not by a perpendicular magnetic field. These predictions are basically confirmed by experiments. Figure 9 shows the wave amplitudes as a function of magnetic field perpendicular to the propagation direction for several frequencies while everything else is kept the same. No wave damping by magnetic field is observed. In contrast, the waves are damped by an imposed magnetic field along the propagation direction, as shown in the single point measurements, Fig. 10. The plotted amplitudes are normalized by the amplitude without magnetic field. It is seen that the wave amplitude is reduced by a factor of 2 when a magnetic field of 500 G is imposed.

Linear theory predicts wave damping by a parallel magnetic field as shown in Eq. (21). The damping rate, given by

$$\exp\left[-\frac{B_{0x}^2\omega k_r}{2\eta(\rho\omega^2+2Tk_r^3)}\Delta x\right], \tag{31}$$

where $\Delta x \simeq 4.1$ cm is the distance between the paddle and the measurement location, is also shown in Fig. 10 as the dotted line. The observed damping rates are much larger than

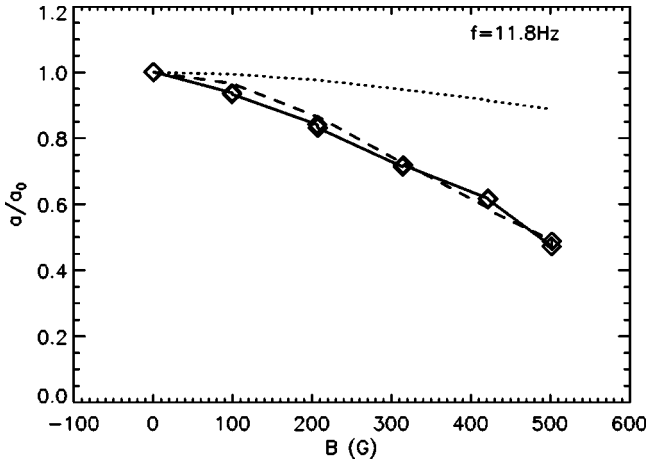

FIG. 10. The wave amplitude measured by the first laser as a function of magnetic field parallel to the propagation direction. The dotted and dashed lines represent predictions by linear theory using actual distance between the paddle and measurement Δx and a distance of $6\Delta x$, respectively.

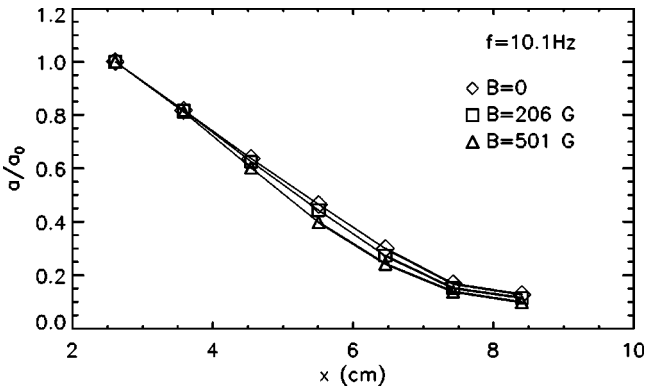

FIG. 11. The normalized wave amplitudes as functions of x for several magnitudes of magnetic field parallel to the propagation direction.

the predictions, but would be consistent with predictions if instead $6\Delta x$ was used in Eq. (31) as also shown in Fig. 10 as the dashed line. Here we need to point out that the wave damping given by Eq. (31) accounts only for the MHD effects during the wave *propagation*, but not for the wave *generation* by the paddle, which is also subject to the MHD interactions. Such MHD effects are well conceivable since the cross-field motions tend to bend the magnetic field lines in a probably nonlinear fashion, although detailed theoretical modeling is beyond the reach of the present linear theory. The observed damping enhancement likely reflects such MHD effects during the wave generation. Note that experiments in water did confirm that the wave driving hardware alone is unaffected by the magnetic field.[19]

Furthermore, the wave damping due to magnetic field parallel to the propagation direction is observed in between the measurements at seven locations. As an example, Fig. 11 shows the normalized wave amplitudes as functions of x for $B=0$, 206 G, and 501 G, respectively. It is clearly seen that the wave is damped more rapidly when a stronger magnetic field is applied. To better quantify the wave damping, measurements at each given magnetic field are fitted to the function shown in Eq. (30) to obtain a spatial damping rate k_i. The results are shown in Fig. 12 as squares. Despite certain scatters in the obtained damping rates, a trend for increased damping rate with magnetic field is apparent. The theoretically predicted damping rates given by Eq. (21) $k_i(B)$ are calculated by using the measured values for all other parameters. Plotted also in Fig. 12 as the dashed line is $k_i(0)+k_i(B)$ where $k_i(0)$ is the measured damping rate at $B=0$. The agreement is reasonable given the scatter and errors in the experimentally determined damping rates.

V. IMPLICATIONS TO FUSION APPLICATION

Given theoretical and experimental results and their physics understanding described in the previous sections, discussions are in order with regard to their implications to the proposed application of a free-surface liquid metal first wall in the fusion reactors.[2–4] Below we discuss two specific effects: magnetic damping of surface waves, and an instability when the Lorentz force is used to support a free-surface liquid metal layer against gravity.

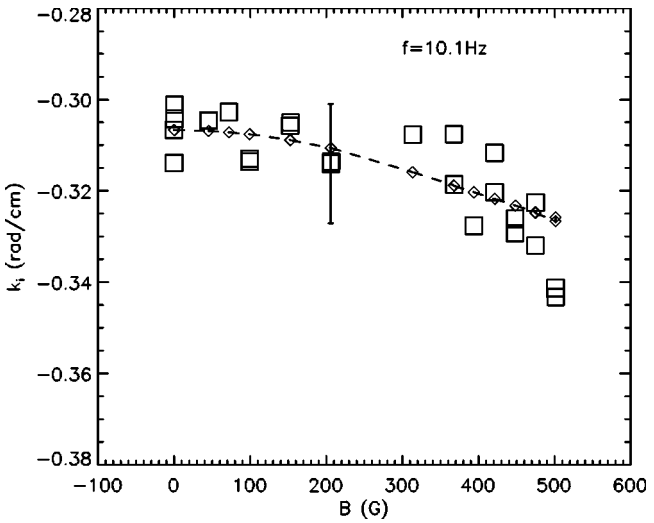

FIG. 12. The wave damping rate (squares) as a function of magnetic field parallel to the propagation direction. The dashed line represents predictions by linear theory (see text).

A. Magnetic damping of surface waves

An important dimensionless parameter here is $\alpha = B^2/\rho\eta\omega$. For a typical magnetic field strength of 10 T in the magnetic fusion reactors, α is much larger than unity unless $f > 100$ kHz for lithium or $f > 10$ kHz for gallium. However, the surface tension becomes important and strongly stabilizing [Eq. (21)] at these high frequencies. Therefore, one expects that the large magnetic fields in the magnetic fusion reactors will stabilize surface disturbances very effectively along the field direction in the deep fluid limit. In addition, a finite vertical magnetic component will further stabilize the surface as shown in previous studies.[15,21,29]

However, there is no magnetic damping on disturbances propagating in a horizontal, but perpendicular, direction, as shown in the previous sections. Even for the case when the disturbances propagate parallel to magnetic field, the damping effect does not exist if the wavelength is much longer than $2\pi h$ so that the liquid is shallow, i.e., $kh \ll 1$. This is seen by taking $\tanh(Kh) \approx Kh$ in Eq. (18) to yield

$$\rho\omega^2 = (\rho g + j_{0y}B_{0x} + k^2T)k^2h,$$

where the damping effect does not appear to first order in kh. Intuitively, this can be understood as waves do not store energy in bending field lines when fluid motion in the vertical direction is suppressed in the shallow limit. If $h = 5$ mm, then the critical wavelength above which there is no large stabilizing effect from magnetic field is about 3 cm. Viscous damping [e.g., Eq. (25)] in the case may become important. Therefore, in the application of a free-surface liquid metal first wall in a fusion reactor, it may not be possible to depend on magnetic damping to suppress disturbances. However, surface conditions, such as existence of an oxide layer, may provide more effective stabilization for possible disturbances, as observed experimentally in the preceding section. Of course, the detailed atomic physics and chemistry, as well as their manifestation as surface tension, need to be understood before they can be better applied in the reactor environment.

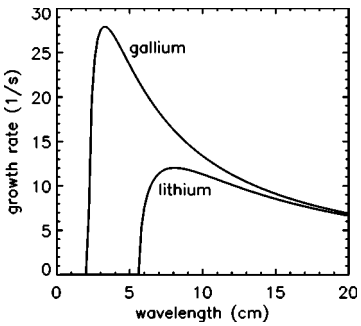

FIG. 13. The growth rate as functions of wavelength for lithium or gallium layer supported by the Lorentz force against gravity in the deep liquid limit.

B. Stability of a liquid metal layer supported by Lorentz force against gravity

In order to completely cover the plasma in a fusion reactor, some parts of a liquid metal layer need to be supported against gravity. One proposed method is to use the Lorentz force by inducing electric current in the liquid metal with an appropriate angle to the background magnetic field so that the resulting Lorentz force is upward to offset the gravity force.[4] This scheme works if the supported liquid metal is stable. However, the obtained dispersion relation, Eq. (18), suggests that this is not the case.

Using the coordinate shown in Fig. 1, now the gravity force ρg points upward and the Lorentz force, $|\boldsymbol{j}_0 \otimes \boldsymbol{B}_0| = |j_{0x}B_{0y} - j_{0y}B_{0x}| \geqslant \rho g$, points downward. Thus the term ρg in Eq. (18) needs to be replaced by $-\rho g$. As discussed in Sec. II D, only one of the two terms of the Lorentz force $j_{0y}B_{0x}$ appears in the dispersion relation. This only term will also disappear when the x direction or the propagation direction is set to be perpendicular to $\boldsymbol{B}_0$. The resultant dispersion relation then becomes

$$\rho\omega^2 = (-\rho g + k^2T)k \tanh(kh), \tag{32}$$

which predicts instability for sufficiently small k or long wavelength. This is essentially the Rayleigh–Taylor instability. Figure 13 shows the growth rates for both lithium and gallium cases. The critical wavelength is determined by the surface tension, which may vary depending on the surface conditions, as described in this paper. The typical growth time is on the order of 0.1 s for lithium, which sets the maximum time scale for the liquid metal to stay in the layer supported by the Lorentz force. This can be translated into a minimum speed with which liquid metal is forced to flow across certain distances in the reactor chamber. For example, for a distance of 1 m, the minimum speed is 10 m/s if only one e-folding time is allowed for this instability to grow. Again, the existence of a surface oxide layer can slow down its growth.

VI. CONCLUSIONS

Effects of magnetic field on small-amplitude surface waves on liquid metal are studied in detail both theoretically

and experimentally in the small magnetic Reynolds number limit. Theoretically, a linear dispersion relation is derived when horizontal magnetic field and electric current is imposed, including effects from surface tension. Waves damp in the deep liquids ($kh \gg 1$) if traveling parallel to the magnetic field. Under a weak magnetic field ($B^2/\rho\eta\omega \ll 1$), waves are weakly damped with no effects on propagation characteristics while in the opposite limit the waves are strongly damped with shortened wavelengths. Experimentally, the planar MHD surface waves on liquid gallium are studied in detail with a weak magnetic field and in the deep liquid limit by using a computer-controlled paddle in a table-top device. Gallium was chosen simply due to its easy use. A noninvasive diagnostic accurately measures surface waves at multiple locations by reflecting an array of lasers off the surface onto a screen, which is recorded by an ICCD camera. The measured dispersion relation is consistent with the linear theory with a reduced surface tension likely due to surface oxidation. It is observed that surface waves are damped when a horizontal magnetic field is imposed parallel to the propagation direction. No damping is observed with a perpendicular magnetic field. These results are in excellent agreement with the linear theory. The existence of a strong wave damping without magnetic field suggests the importance of the surface oxide layer. Implications to the liquid metal wall concept in fusion reactors are discussed. Magnetic damping can suppress surface disturbances with short wavelengths propagating along the magnetic field, but waves with long wavelengths or propagating across magnetic field are unaffected. A liquid metal layer supported by the Lorentz force against gravity is unstable to the Rayleigh–Taylor instability when a perturbing wave vector is perpendicular to the magnetic field and its wavelength is sufficiently long, possibly leading to a practical limitation of these applications.

ACKNOWLEDGMENTS

The authors are indebted to Dr. S. Zweben for his initiatives and contributions, Dr. R. Kulsrud for his insights on the wave theory, Dr. M. Yamada for his encouragements, A. Paterson for his technical assistance, G. Brumfiel, and L. Bell for their numerous contributions under the National Undergraduate Fellowship program. This work was supported by the U.S. Department of Energy.

[1] E. Northrup, Phys. Rev. **25**, 474 (1907).
[2] S. Molokov and C. Reed, "Review of Free-surface MHD Experiments and Modeling," Argonne National Laboratory Technical report, ANL/TD/TM99-08, 1999, National Technical Information Service Document No. DE2001757509 (unpublished).
[3] N. Morley, S. Smolentsev, L. Barleon, I. Kirillov, and M. Takahashi, Fusion Eng. Des. **51–52**, 701 (2000).
[4] M. Abdou, A. Ying, N. Morley *et al.*, Fusion Eng. Des. **54**, 181 (2001).
[5] L. Zakharov, Phys. Rev. Lett. **90**, 045001 (2003).
[6] H. Rappaport, Phys. Plasmas **8**, 3620 (2001).
[7] J. Melcher, Phys. Fluids **4**, 1348 (1961).
[8] G. Murty, Ark. Fys. **19**, 499 (1961).
[9] S. Breus, Sov. Phys. Tech. Phys. **5**, 960 (1961).
[10] G. Murty, Ark. Fys. **19**, 483 (1961).
[11] J. Shercliff, J. Fluid Mech. **38**, 353 (1969).
[12] R. Baker, Nature (London) **207**, 65 (1965).
[13] M. Duc, C.R. Acad. Sci., Paris. Serie A **266**, 738 (1968).
[14] J. C. Rook, Ph.D. thesis, Massachusetts Institute of Technology, 1964.
[15] A. Shishkov, Magnetohydrodynamics (N.Y.) **28**, 368 (1992).
[16] V. Korovin, Tech. Phys. **41**, 752 (1996).
[17] M. Schaffer, J. Fluid Mech. **33**, 337 (1968).
[18] L. Landau and E. Lifshitz, *Fluid Mechanics* (Butterworth Heineman, Oxford, 1987).
[19] W. Fox, "Magnetohydrodynamic surface waves in liquid metal," Bachelor thesis, Princeton University, 2001.
[20] T. Iida and R. Guthrie, *The Physical Properties of Liquid Metals* (Clarendon, Oxford, 1988).
[21] B. Lehnert, Ark. Fys. **5**, 69 (1952).
[22] T. Cowling, *Magnetohydrodynamics* (Interscience, New York, 1957).
[23] D. Lide, *CRC Handbook of Chemistry and Physics* (CRC, Boca Raton, 2002).
[24] E. Falcon, C. Laroche, and S. Fauve, Phys. Rev. Lett. **89**, 204501 (2002).
[25] M. Regan, E. Kawamoto, S. Lee, P. Pershan, N. Maskil, M. Deutsch, O. Magnussen, N. Ocko, and L. Berman, Phys. Rev. Lett. **75**, 2498 (1995).
[26] J. Penfold, Rep. Prog. Phys. **64**, 777 (2001).
[27] J. Allen and S. Rice, J. Chem. Phys. **67**, 5105 (1977).
[28] M. Regan, H. Tostmann, P. Pershan, O. Magnussen, E. DiMasi, N. Ocko, and M. Deutsch, Phys. Rev. B **55**, 10786 (1997).
[29] L. Fraenkel, J. Fluid Mech. **7**, 6 (1959).